Science of the Total Environment 721 (2020) 137629

Contents lists available at ScienceDirect

Science of the Total Environment

journal homepage: www.elsevier.com/locate/scitotenv

Real time detection and characterisation of bioaerosol emissions from wastewater treatment plants

Jiang-han Tian [a], Cheng Yan [b,a], Zaheer Ahmad Nasir [a,*], Sonia Garcia Alcega [c], Sean Tyrrel [a], Frederic Coulon [a]

[a] School of Water, Energy and Environment, Cranfield University, Cranfield MK43 0AL, UK
[b] School of Environmental Studies, China University of Geosciences, Wuhan 430074, PR China
[c] School of Physical Sciences, The Open University, Walton Hall, Milton Keynes MK6 7AA, UK

HIGHLIGHTS

- Real time bioaerosols monitoring at wastewater treatment plant (WWTP) by Spectral Intensity Bioaerosol Sensor (SIBS)
- Highly variable bioaerosol emissions were observed at WWTP and background site.
- Fluorescence spectra were multimodal with distinctive features at two sampling sites.
- Similarity between SIBS spectra and wastewater excitation-emission matrix
- SIBS can contribute to enhancing selectivity for characterisation of bioaerosols.

GRAPHICAL ABSTRACT

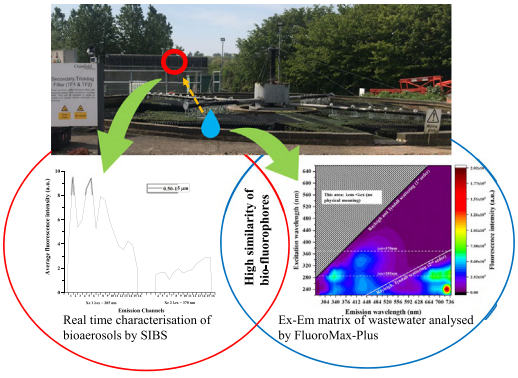

ARTICLE INFO

Article history:
Received 21 January 2020
Received in revised form 27 February 2020
Accepted 27 February 2020
Available online 29 February 2020

Editor: Damia Barcelo

Keywords:
Bioaerosols
Real-time monitoring
Wastewater treatment plant
Spectral Intensity Bioaerosol Sensor
Fluorescence spectra

ABSTRACT

Bioaerosol emissions from wastewater treatment plants may pose adverse health impact on workers and nearby communities. To detect and characterise bioaerosol emissions from wastewater treatment plant (WWTP), a novel real-time bioaerosol sensor, Spectral Intensity Bioaerosol Sensor (SIBS) was employed at a WWTP and a background site. The SIBS records a range of data (size, shape, and fluorescence emission across 16 wavelength bands from 298 to 735 nm for two excitation wavelengths (285 nm and 370 nm)) on single particles in real time. Additionally, excitation-emission matrix (EEM) of wastewater samples obtained by a spectrofluorometer was compared with SIBS spectra from WWTP. The results showed that the average number concentrations of total particles (NT) and fluorescence particles (NF) were both higher at the WWTP (NT = 2.01 cm^{-3}, NF = 1.13 cm^{-3}) than the background site (NT = 1.79 cm^{-3}, NF = 1.01 cm^{-3}). The temporal variation of NF and NT was highly variable at the WWTP and the concentration peaks were consistent with on-site activities. Moreover, the time-resolved number-size distribution of fluorescent particles revealed the predominance of fine scale particles (<1 μm) and the time-series channel by channel number concentrations demonstrated the temporal variability of dominant bio-fluorophores. Furthermore, the overall and size-segregated fluorescence spectra at two sites were multimodal. In particular, the fluorescence intensity increases with increasing particle size in WWTP spectra, which is not present in the background spectra. In addition, the highly resolved SIBS fluorescence spectra were broadly similar to EEM of wastewater. These findings confirmed that the spectrally resolved fluorescence detected by SIBS is capable of providing reliable bio-fluorophores information of bioaerosol emissions generated from wastewater, thus holding the potential for better characterisation of bioaerosols in real time.

* Corresponding author.
E-mail address: z.a.nasar@cranfield.ac.uk (Z.A. Nasir).

https://doi.org/10.1016/j.scitotenv.2020.137629

1. Introduction

The world's increasing population and urbanisation processes exacerbate wastewater generation (IWA, 2018). Thus, there is a growing number of wastewater treatment plants (WWTPs) to ensure safe inland discharge, disposal and reuse (Mateo-Sagasta et al., 2015; IWA, 2018; Korzeniewska, 2011). Different WWTP operations may lead to aerosolization of diverse biological materials (Michałkiewicz, 2019; Pascual et al., 2003; Rizzo et al., 2013), capable of allergenic, infectious or toxic potential, leading to growing concerns of potential health risks to the sewage workers and nearby communities (Gerardi and Zimmerman, 2004; Fracchia et al., 2006; Korzeniewska et al., 2008; Prazmo et al., 2003; Fracchia et al., 2006). Understanding the concentration, distribution, composition and resultant impact of bioaerosols is critical to elucidate the potential risks of public health, especially on occupational exposure at WWTP (Swan et al., 2003). Consequently, there is an increasing interest in the detection and characterisation of bioaerosol emissions from WWTPs.

Traditional bioaerosol sampling approaches with a range of off-line post-collection analysis for bioaerosol monitoring (culture-based and culture-independent) can only provide snapshot data with poor time resolution (hours to days), poor repeatability and are labour intensive (Korzeniewska, 2011; Griffiths and Decosemo, 1994; Chi and Li, 2007; Heidelberg et al., 1997), which cannot capture the true nature and magnitude of bioaerosol emissions from a source. Thus, there is a need for rapid bioaerosols detection and characterisation methods to advance bioaerosol risk assessment and management from environmental sources including WWTPs (Nasir et al., 2019).

In recent years, advancements in laser-induced fluorescence (LIF) spectroscopy techniques have contributed to the application of qualitative and quantitative studies of bioaerosols in real time (Pöhlker et al., 2012; Després et al., 2007; Bowers et al., 2009; Fröhlich-Nowoisky et al., 2009; Garcia-Alcega et al., 2017; Garcia-Alcega et al., 2018; Ferguson et al., 2019). It is based on the principle that a specific organic molecule of biological origin (e.g. proteins, coenzymes, structural compounds, pigments) exhibits intrinsic fluorescence (or autofluorescence) (Pöhlker et al., 2012; Pan, 2015). In general, a given fluorophore usually characterised by the excitation (λex) and emission wavelengths (λem), while excitation-emission matrix (EEM) could enhance the qualitative assignment of spectral modes to known fluorophores, providing insight into molecular origin of fluorescence accordingly (Miao et al., 2003). The ultraviolet aerodynamic particle sizer (UV-APS) and Wideband Integrated Bioaerosol Sensor (WIBS) series are LIF-based instruments which have been utilised in continuous measurement of bioaerosols in urban area (e.g. Huffman et al., 2010), industrial processes (O'Connor et al., 2015; Li et al., 2016), high altitude (Crawford et al., 2016; Gabey et al., 2013; Perring et al., 2015; Ziemba et al., 2016; Yue et al., 2019) etc. for many years, but their application is relatively rare in WWTP. However, the broad emission detection bands of UV-APS and WIBS make it difficult to precisely classify among different categories of bioaerosols (Pöhlker et al., 2012; Nasir et al., 2019). In addition, the complexity of the molecular components and non-biological interferents that fluoresce (e.g. mineral dust, polycyclic aromatic hydrocarbons, secondary organic aerosol) in a natural environment also impede their application (Pöhlker et al., 2012).

Lately, building on the WIBS, an upgraded device with highly resolved fluorescence intensity measurements known as the Spectral Intensity Bioaerosol Sensor (SIBS) has been developed by Droplet Measurement Technologies Inc. (Longmont, USA). The WIBS measures fluorescence emission in three emissions (λem) bands for two excitation wavelengths (λex = 280 nm and 370 nm) as follows: FL1: λex = 280 nm, λem ~ 310–400 nm, FL2: λex = 280 nm, λem ~ 420–650- nm, and FL3: λex = 370 nm, λem ~ 420–650 nm. In contrast, SIBS uses dual excitation wavelengths (λex = 285 nm and λex = 370 nm) and provides measurements of size, shape and spectrally resolved fluorescence in 16 channels (λem = 298–735 nm) at two excitation wavelengths (Nasir et al., 2018; Könemann et al., 2019; Nasir et al., 2019). Thus, highly resolved fluorescence spectral information offered by SIBS in comparison to WIBS can improve the selectivity to discriminate and classify bioaerosol emissions. An earlier study by Nasir et al. (2019) demonstrated that SIBS offered additional spectral information to the WIBS (Nasir et al., 2019). However, the resolved emission spectra require meaningful interpretation in terms of assigning spectral responses to bio-fluorophores. Based on the available literature on excitation and emission matrix spectra of atmospherically relevant biological fluorophores (Hernandez et al., 2016; Pöhlker et al., 2012; Pan et al., 2010; Hill et al., 2009), a tangible explanation of the molecular origin of fluorescence in different emission channels in SIBS could be deduced.

In the present study, the SIBS was used to detect and characterise the bioaerosol emissions from a WWTP and compared with the background environment. Furthermore, the fluorescence spectra provided by SIBS and the wastewater EEM analysed by a spectrofluorometer were compared to evaluate the extent to which the highly resolved fluorescence intensity measurements by SIBS could be used to characterise bioaerosol emissions from wastewater treatment.

2. Materials and methods

2.1. Sampling procedure

Samplings were conducted at the WWTP (coordinate: 52°04′45.3″N 0°37′35.3″W) and the campus background site (coordinate: 52°04′ 22.4″N 0°37′37.4″W) at Cranfield University, UK (Fig. 1). The background site was chosen as a control site with significantly different emission sources in comparison to WWTP. For each site, five measurements were carried out during daytime at a height of 1 m by SIBS, and on-site activity was recorded during each sampling period. A general description of the two sites and sampling strategy are provided in Table 1.

Additionally, five wastewater samples were collected from the trickling filter (TF) ponds at the WWTP with a sterile 15 ml conical centrifuge tubes (Falcon™) at the end of each sampling day. The wastewater samples were stored in the fridge at 4 °C before being analysed by the spectrofluorometer FluoroMax®-Plus (HORIBA JOBIN YVON INC, USA) in the laboratory. The meteorological data were provided by Kisanhub Weather Station Network located in the university campus and the WWTP.

2.2. Instrumentation and analysis

2.2.1. Spectral Intensity Bioaerosol Sensor (SIBS)

The detailed information about the operation principle of SIBS was comprehensively described by Nasir et al. (2019) and Könemann et al. (2019). Briefly, SIBS records single-particle fluorescence spectrum across 16 emission wavelength bands (from 298 to 735 nm) at two excitation wavelengths (λex = 285 nm and 370 nm) along with size and shape in real time. The wavelength ranges of 16 fluorescence emission channels are listed in Table 2.

SIBS records size, shape and fluorescence emission intensity across different channels for single particles as HDF5 format. These files were imported into a data analysis toolkit (SIBS Toolkit) for offline data analysis. An averaging interval of 60 s and particle size limit of 0.50–15 μm was chosen when processing for the total and size segregated (15 bins) number concentration time-series data. The background fluorescence signal of SIBS was recorded by running a Forced Trigger (FT) mode prior to each measurement, involving sample pump off and the xenon lamps firing at an interval of 150 ms. A minimum of 5 min forced trigger data was recorded before each measurement at a site. This 'Forced Trigger' fluorescence emission intensity data was used to set a lower fluorescence threshold to determine fluorescent particles. In this study, the mean + 3 × standard deviation (σ) of emission fluorescence intensity in each channel was applied to define the fluorescent FT

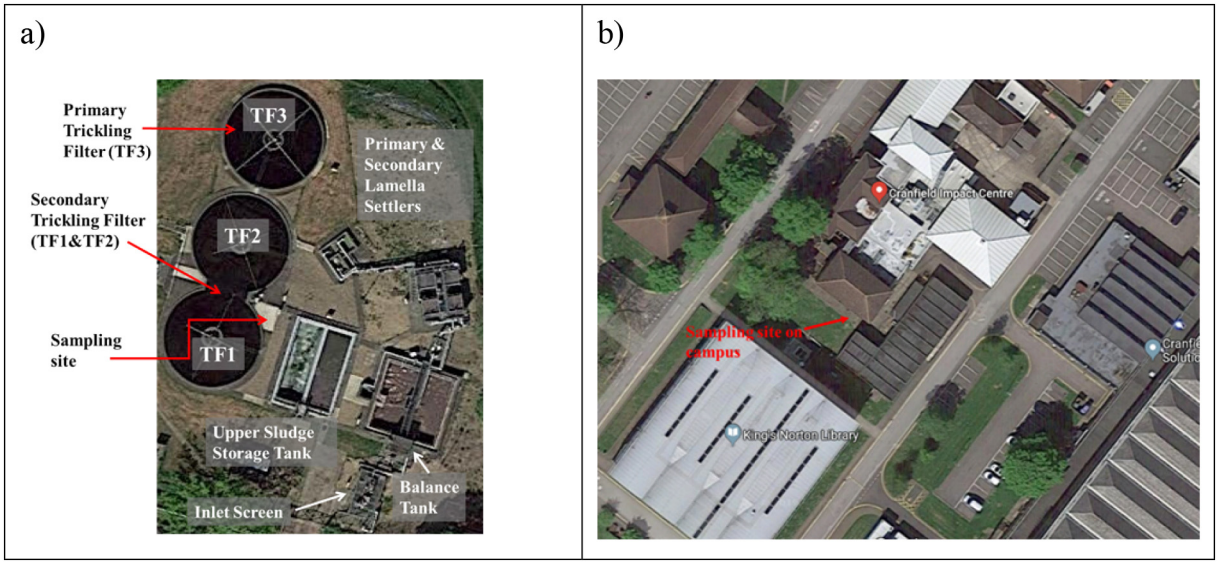

Fig. 1. The location of sampling sites in the wastewater treatment plant (a) and university campus (b).

threshold value for each channel. In addition, two xenon flash lamps were recharged for a very short time, so some particles might have not been flashed (excited). Hence, three particle categories were obtained: total particles, excited particles and fluorescent particles. Eq. (1) was used for correcting the number concentration of fluorescence particles:

$$\textbf{Fluorescentparticle conc.} = \frac{\mathbf{F}}{\mathbf{E}} \times \mathbf{T} \quad (1)$$

where T, E, F refer to the number concentrations (#/cm^3) of total, excited and fluorescent (calculated from fluorescent threshold value of FT data) particles (Nasir et al., 2018; Nasir et al., 2019). # denotes the number of particles.

Fluorescence spectra of each measurement at WWTP and background site were calculated from excited particle by particle emission intensity values minus FT threshold values (mean + 3σ) across each channel, followed by the calculation of mean fluorescence intensity within each emission channel for two excitation wavelengths. Finally, a mean fluorescence spectrum was calculated for each site. Additionally, size fractionated fluorescence spectral profiles were also calculated by grouping fluorescent particles into five size ranges: 0.5–1, 1–2.5, 2.5–4, 4–10 and 10–15 μm.

Table 1
Description of the sampling sites and sampling strategy.

Site	Description	Sampling strategy
Background	A grassed area with mature trees nearby; surrounded by university campus buildings	• Sampling conducted at the grass plot at Cranfield University (Fig. 1b). • Five repeated measurement periods for 3–3.5 h during daytime. • Sampling on 27th, 28th and 29th June 2019 and 1st and 2nd July 2019 (labelled as day 1, day 2, day 3, day 4 and day 5 in the Results and discussion section)
WWTP	A trickling filter based WWTP treating domestic wastewater and storm drains within the campus with a daily capacity of 450 m^3; surrounded by agricultural fields and woodland	• Sampling between the secondary trickling filter beds (TF1) and the upper sludge storage tank (Fig. 1a) • Five repeated measurement periods for 4 h during daytime each. • Sampling on 15th, 22nd, 29th, 30th and 31st May 2019 (labelled as day 1, day 2, day 3, day 4 and day 5 in the Results and discussion section)

2.2.2. FluoroMax®-Plus: Bench-top spectrofluorometer

Two milliliters of each wastewater sample were transferred into a cuvette which was then placed in the sample chamber of FluoroMax®-Plus. Three repeated measurements of variable excitation wavelength from 220 to 650 nm (increment = 20 nm), emission wavelength from

Table 2
Fluorescence measurement channels (Ch) and wavelength ranges.

Channel	Lower wavelength (nm)	Upper wavelength (nm)
1	298.2	316.4
2	316.4	344.8
3	344.9	362.5
4	377.5	401.5
5	401.5	429.7
6	430.2	457.5
7	456.7	485.6
8	486.0	514.0
9	514.1	542.0
10	542.0	569.8
11	569.9	597.6
12	597.6	625.2
13	625.3	652.8
14	652.8	680.2
15	680.3	707.5
16	707.5	734.7

270 to 740 nm (increment = 5 nm) and fluorescence intensity were employed for each wastewater sample. The increment in a wavelength scan is the spacing between adjacent data points which affected the resolution of the spectrum and total time for data acquisition. Considering the instrument's spectral response and influence of the light-absorbance properties of the wastewater sample, 20 nm increment of λex and 5 nm increment of λem was selected (Horiba, 2009; Gilmore, 2011). Calibration was carried out prior to each operation. The spectral data were acquired when the analysis finished. The entire process was controlled by the FluorEssence™ software with Origin® embedded for graphic presentation. The correction including dark offset, blank subtraction and correction-factor file were activated in FluorEssence™ software and applied automatically on the excitation-emission matrix (EEM) spectra by following the equation: Scorrected (or Sc) = (Smeasured − Sdark − Sblank) × Correction-factor file (Horiba, 2012). Thus the emission intensity showing on the EEM contour map was S1c/R1c (corrected fluorescence emission intensity). First and second order Rayleigh scattering was masked in order to avoid the influence of distorted sharp peak of fluorescence intensity caused by elastic scattering and second order effect (Pöhlker et al., 2012).

3. Results and discussion

3.1. Number concentrations

3.1.1. Average particle number concentrations

The average number concentrations of total particles (NT) and fluorescence particles (NF) at WWTP (NT = 2.01 cm^{-3}, NF = 1.13 cm^{-3}) were both higher than the background site (NT = 1.79 cm^{-3}, NF = 1.01 cm^{-3}) (Table 3). A non-parametric Mann-Whitney *U* test has been undertaken to test the difference in total particles (NT), fluorescent particles (NF) and ratio (NF/NT) between the WWTP and the background site. There was a statistically significant difference between WWTP and the background concentration of NT and NF ($p < 0.05$). Furthermore, there was a larger variation in the fluorescent particle fractions (ratio of NF/NT) at the WWTP site (from 0.42 to 0.85) compared to the background site (from 0.55 to 0.68). The coefficient of variation (the ratio of the standard deviation to the mean) also illustrated a larger variability in NF and NT at the WWTP site. However, there was no statistically significant difference between the ratio (NF/NT) at WWTP and background site. This finding, keeping in view the larger variation in the fluorescent particle fraction at the WWTP suggested that while the average ratios of fluorescent particles at two sites do not differ significantly, NF are more dynamic and affected by on-site operations and activities around WWTP leading to intermittent higher fluorescent fraction (up to 0.85). Hence, real-time sampling holds the potential to quantify the temporal variability of bioaerosol emissions at the WWTPs.

Table 3
Descriptive statistics of particle concentrations at the wastewater treatment plant and the background site.

		Number concentration		Ratio
	Parameter	NT (cm^{-3})	NF (cm^{-3})	NF/NT
WWTP	Average	2.01[a]	1.13[b]	0.57
	Max	5.84	4.97	0.85
	Min	0.36	0.21	0.42
	CV (%)	54	54	10
Background	Average	1.79[a]	1.01[b]	0.56
	Max	3.99	2.66	0.68
	Min	0.27	0.14	0.55
	CV (%)	41	43	6.0

NT = number concentrations of total particles, NF = number concentrations of fluorescent particles, ratio of NF/NT = fluorescent fractions, CV = coefficient of variation. The values with the same superscript were significantly different at the 0.05 level of significance (a, b).

The particle number concentrations in this study were higher in comparison to previous work at the same WWTP by Nasir et al. (2019) (NT = 1.03 cm^{-3}, NF = 0.25 cm^{-3}). This was likely due to differences in the chosen particle size ranges. The particle size reported by Nasir et al. (2019) was 0.5–7 μm, while the particle size range for this study was 0.5–15 μm.

3.1.2. Temporal variation of particle number concentrations

Fig. 2 shows the temporal variation of particle number concentrations at the WWTP and the background sites. The meteorological data are provided in Table S1. While, the NF and NT were variable at both sampling sites, the levels were higher at the WWTP in comparison to the background site. Specifically, the fluctuation of particle number concentration was most obvious on day 4 at the WWTP (Fig. 2a), which corresponded to high and variable wind speed on that day (Table S1). This may have contributed to the aerosolization of wastewater. Furthermore, most of the particle concentration peaks were consistent with the daily records, which is mowing activity (13:20 on day 1, and 14:20–14:50 on day 4), sludge dredging (at 12:00 and 12:45 on day 2) and tank flushing (9:30–9:50 on day 4, and 9:50 on day5). Additionally, sharp peaks in particle number concentrations observed during the afternoon on day 1 (15:00), day 4 (14:00) and day 5 (14:20) could be due to high flow of wastewater to tricking filters leading to increased aerosolization (Table S2).

The peak of NT and NF at the background site (Fig. 2b) were related to the exhaust fan operation, vehicular activities and wind-blown materials nearby the sampling site (Table S2). The highest concentration was recorded on day 2, since there was a continuous fuel burning smell originating from Cranfield airport and this along with high wind speed had probably resulted in high NT and NF.

These results indicate that the fluorescent aerosol emissions were largely affected by the on-site operation and activities, and highlight that "snapshot" sampling methods could not capture the true magnitude and variation of bioaerosol emissions from environmental sources (Nasir et al., 2019).

Apart from that, temperature, relative humidity and solar radiation were reported to be the major influential factors on the level of concentration of bioaerosols in the cultivation methods (Forde et al., 2018; Zhong et al., 2016; Kowalski and Pastuszka, 2018). Generally, with an increase of solar radiation intensity, the concentration of bioaerosols was lower because of the biological sensitivity to sterilization by UV light (Kowalski and Pastuszka, 2018). However, there is no clear relationship between temperature, solar radiation, relative humidity and fluorescent particle concentrations in this study (Table S1). This was because the detection and quantification by SIBS is based on intrinsic fluorescence from biological fluorophores regardless of viability status of airborne biological materials.

3.1.3. Time-resolved number-size distribution of fluorescent particles

Fig. 3 illustrates the number-size distribution of fluorescent particles at the WWTP and the background site. The majority of fluorescent particles were <1 μm (fine particle), which indicated that a large fraction of detected particles consists of submicron biological materials. Shifts in particle size and noticeable fluctuations of particle concentrations were observed over different measurement days at both sites. These variations correspond to the activities discussed previously. Particularly, during day 1 at 15:00 and day 4 at 14:00, there were obvious increases in particle size up to 4.31 μm and 9.57 μm at the WWTP (Fig. 3a). These corresponded to a higher flow of wastewater in the trickling filter. Similarly, on day 2 at 12:00 and 12:45, sludge dredging, and tank flushing happened when particle size went up to 4.83 μm. Finally, on day 4 at 14:00, the particle size had significantly increased up to 7 μm during the mowing activity. Another comparable study by Li et al. (2016) measured the bioaerosol levels and size distribution at a WWTP in Beijing by using UV-APS. Their results showed the predominant fluorescent particle size were centred on 3–4 μm among seven intra-plant sampling sites, which was explained

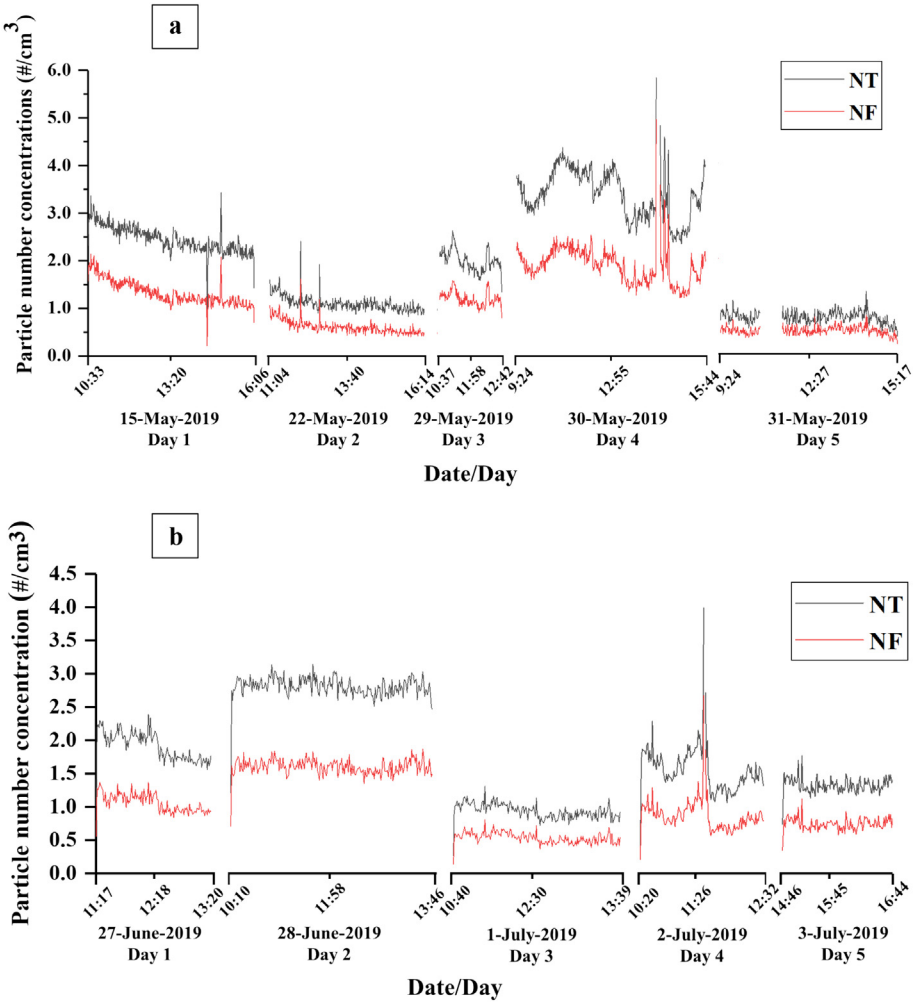

Fig. 2. Temporal variation of total and fluorescent particle number concentrations at (a) wastewater treatment plant and (b) background site (NT = number concentrations of total particles; NF = number concentrations of fluorescent particles).

by the dominance of fungal species or bacterial aggregates. This is probably because UV-APS utilises a single excitation (355 nm) and emission band (420 to 575 nm) to detect fluorescence particles. Therefore, the fluorescent particles may have escaped from the detection comparing to dual wavelength excitation and multi-channel emission measurements of SIBS. Furthermore, discrimination of the fluorescent particles is significantly influenced by the applied fluorescence threshold (Healy et al., 2014; Huffman et al., 2012; Huffman et al., 2019).

At the background site (Fig. 3b), the fine particles were also predominant across the five sampling days and the variations corresponded to the activities observed and discussed earlier. The fluorescent particle concentration at this site was primarily influenced by local sources such as windblown dust and organic matter, vehicular and fossil fuel emissions from university airport and exhaust from buildings.

The information on particle size distribution is important to understand and predict aerodynamic behaviour, survival, dispersal and potential deposition site of particles in the human respiratory system (Galès et al., 2015; Clauß, 2015), as well as classification and/or discrimination of bioaerosols. The finding of the predominance of fluorescent particles in fine size fraction (below 1 μm) is in line with Nasir et al. (2019). However, it is important to have certainty that the origin of fluorescence in this fraction is from biological materials rather than non-biological interfering compounds (soot, PAH). In order to elucidate the potential fluorophores in particles <1 μm, size fractionated fluorescence spectra were analysed (Section 3.2.2).

3.1.4. Channel by channel particle number concentrations

Figs. 4 and 5 provide the time series of the channel by channel number concentrations of fluorescent particles. At the WWTP, Ch7 and Ch9 of Xe1 were predominant channels on day 1–3 and 5, while Xe1Ch16 was absent during the five-day sampling period (Fig. 4). Specifically, Ch7, Ch9 of Xe1 and Ch7 of Xe2 showed uniform concentration during day 1, while a readily apparent alteration in concentrations were observed at 15:00 (Ch4–5, Ch9, Ch13, Ch16 of Xe2) (Fig. 4a) which is in agreement with the higher flow rate of wastewater activity at the WWTP. Similarly, Ch7 and Ch9 of Xe1 were persistently present on day 2, but absent in Ch1, Ch3, Ch16 of Xe1, and Ch4, Ch5 and Ch10 of Xe2. The concentrations shifted at 12:10 (Ch2–15 of Xe1, Ch7 and Ch11–12 of Xe2) and 12:45 (Ch4–15 of Xe1, Ch7 and Ch9 of Xe2) being consistent with sludge dredging and tank flushing activities (Fig. 4b). Ch6–10 of Xe1 were dominant channels on day 3, but varied at 11:10 (Ch4–5 of Xe1, Ch5, Ch8, Ch12–15 of Xe2), 12:10 (Ch4–5, Ch11–14 of Xe1, Ch11–16 of Xe2) and 12:30 (Ch4–12 of Xe1) (Fig. 4c). Ch2, Ch5 and Ch7 of Xe1 were only exhibited during 10:30–13:00 as the most sustained channels (Fig. 4d). Similarly, Ch2, Ch4–10 of Xe1 and Ch4, Ch10, Ch13, Ch15 of Xe2 were predominant channels on day 5 (Fig. 4e). The blank area between 10:40 and 11:25 signifies the sampling interruption caused by raining (Fig. 4e). Afterwards, the emission channels were dominated by Ch2 and Ch4–15 of Xe1. While there were some channels exhibiting uniform concentration, the

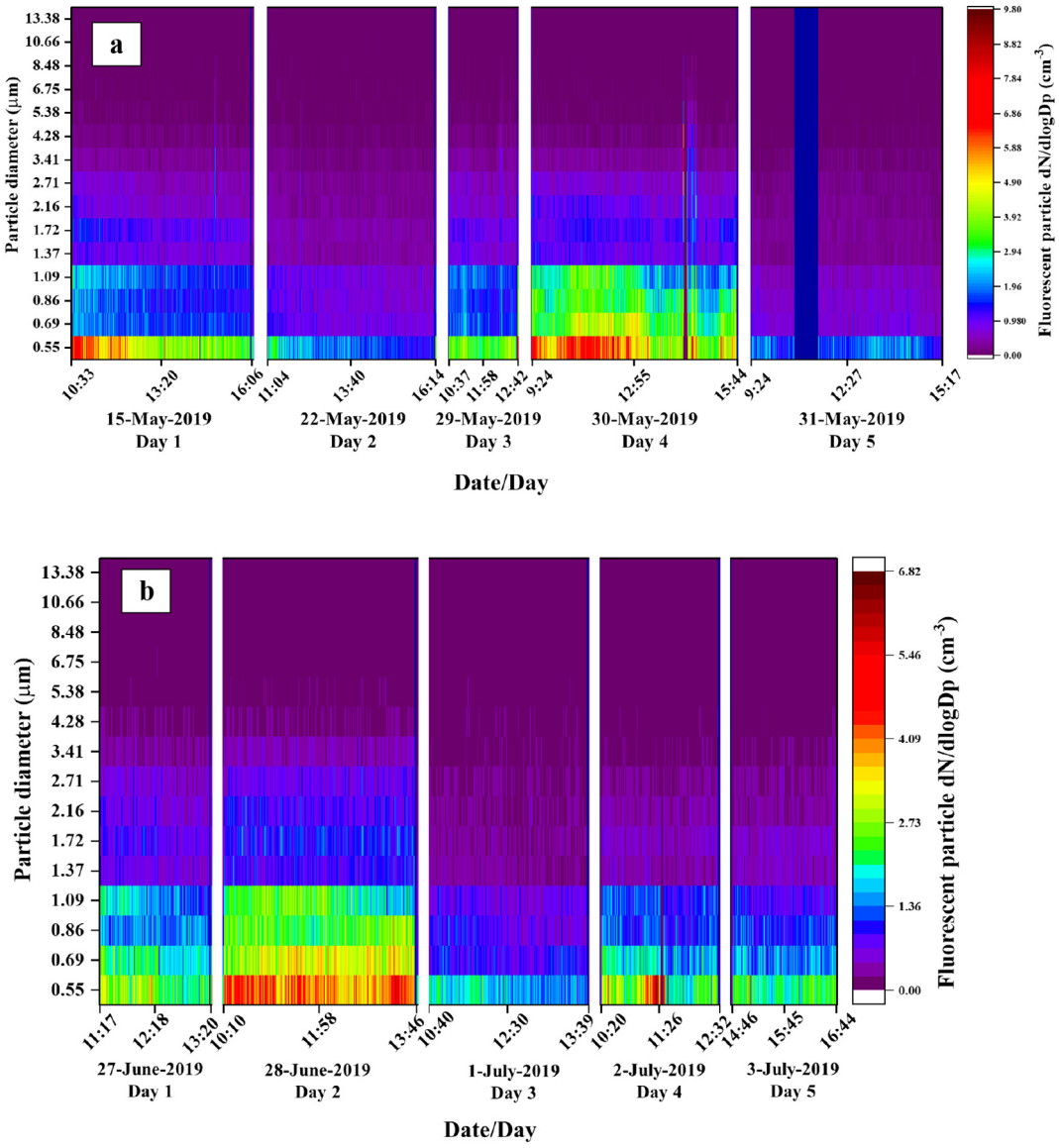

Fig. 3. Time-resolved (1 min) number-size distribution of fluorescent particles at (a) the wastewater treatment plant and (b) the background site.

shifts in concentration to other emission channels were recorded during site-specific activities.

In contrast to the WWTP, Ch11–15 of Xe2 exhibited high number concentrations among five days, while Ch14–16 of Xe1 and Ch10 of Xe2 showed the lowest number concentrations at background site (Fig. 5). Several changes in emission channels agreed with on-site sampling record. For instance, a significant increase in particle number concentrations happened at 11:30 on day 4 showing highest on Ch4 and Ch7–13 of Xe1 and Ch12–15 of Xe2 (Fig. 5d). This peak was probably caused by the sudden opening of a ventilation fan of a nearby air conditioning unit which contributed to the disturbance of airborne particles near the sampling site. Nevertheless, there were no distinct changes in channels in any time duration on day 2 and day 5 at the background site, but higher concentrations were in Ch1–9 of Xe1 and Ch4–16 of Xe2 (being highest concentration on Xe1Ch7) on day 2, and Ch1–2, Ch4–12 of Xe1, Ch4–9 and Ch11–16 of Xe2 on day 5 (Fig. 5b and e).

The predominant channels, along with the assignment of potential atmospheric bio-fluorophores based on the fluorescence emission intensities in each channel, can be used to further characterise temporal variability of bioaerosols based on potential bio-fluorophore from a source. The observed trends in concentration profile of fluorescent particles across different channels and their qualitative assignment to SIBS relevant fluorophores (present in Section 3.2) implied that plant alkaloids, terpenoids, phenolics (secondary metabolites-like), sporopollenin, lignin (structural compound-like), cellular age-related pigments, flavonoids, lipofuscin and ceroid (pigment-like), pteridine nucleotides (cofactors, coenzymes, vitamins-like) fluorophores were generally exhibited at the WWTP. However, tryptophan (amino acid-like), vitamin B6 compounds, pteridine compounds (coenzymes-like), chitin, cellulosic materials (structural compound-like), structurally smaller alkaloids (secondary metabolites-like), chlorophylls (pigments-like) were only assigned to the mowing activity period. These fluorophores are likely to originate from fungal spores, various bacteria and insects' fragments in the ambient air, and grass pollen was the main bioaerosol sources during the mowing activity. Moreover, CaDPA was only present during sludge dredging activity, which was considered to be a unique component of bacterial endospores, thus has been used for spore detection (Pöhlker et al., 2012; Bronk et al., 2000).

The prominent fluorophores at the background site could be assigned to flavonoids, chlorophylls a, b and bacterio-chlorophylls (pigment-like), sporopollenin (structural biopolymers-like), terpenoids (secondary metabolites-like), which mainly stemmed from pollen/plants, bacteria, fungi spores and their cellular fragments. Furthermore, PAHs and HULIS were found to be the potential non-biological

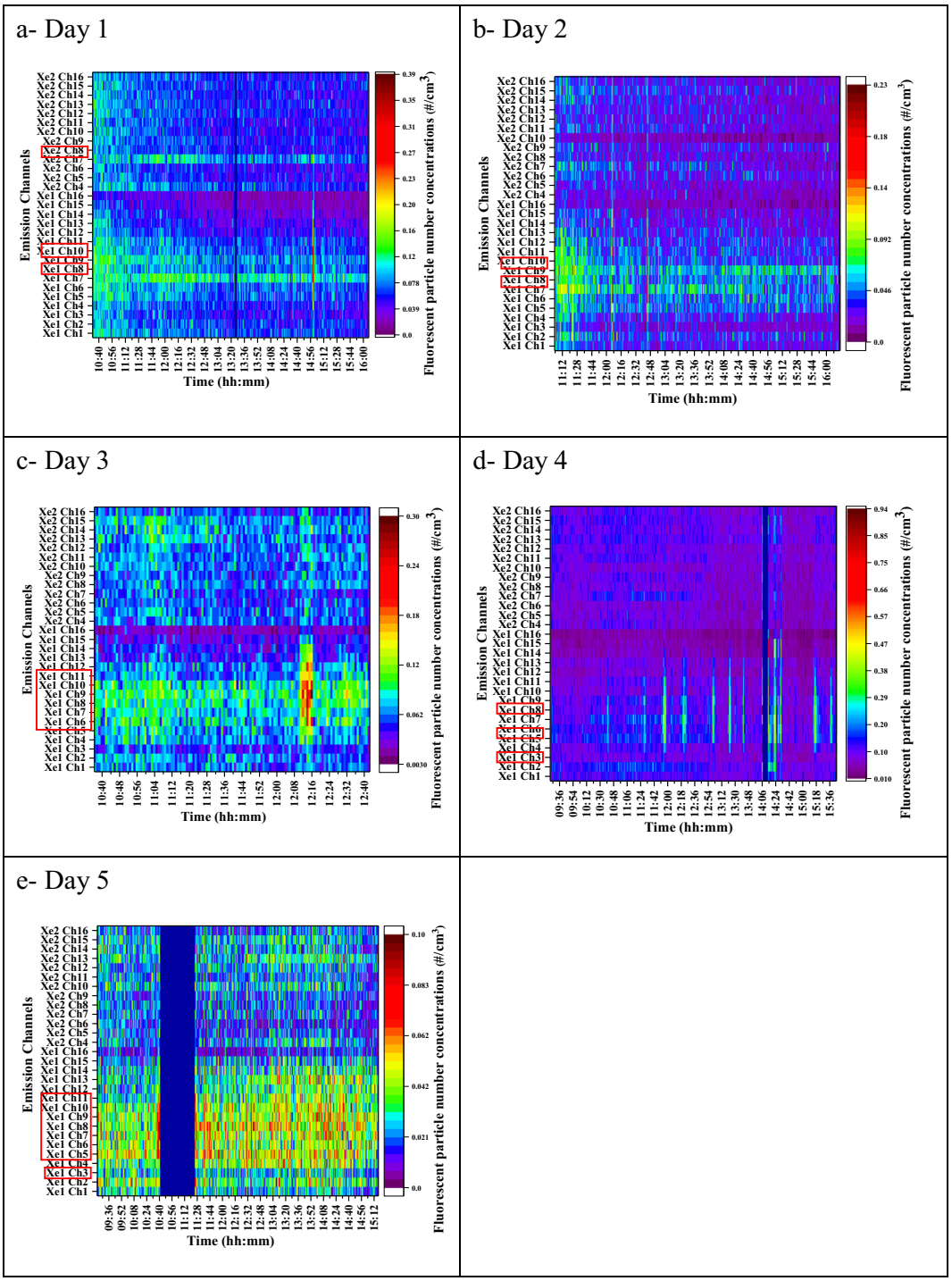

Fig. 4. Channel by channel number concentrations of fluorescent particles at the WWTP.

interferents possibly generated from vehicular emissions and wind-blown organic matter.

3.2. Fluorescence spectra

3.2.1. Overall fluorescence spectra of WWTP and background site

The overall fluorescence spectra (0.50–15 μm) at both sites are presented in Fig. 6. The sample size of the fluorescent particles (0.50–15 μm) for the analysis of fluorescence spectra is summarised in Table 4.

Overall, the fluorescence emission intensity at λex = 285 nm (Xe 1) showed a tendency to be higher than those at λex = 370 nm (Xe 2). This finding corresponds to the findings of Könemann et al. (2019) and is also comparable to multiple WIBS studies (e.g., Hernandez et al., 2016; Perring et al., 2015; Savage et al., 2017). The overall and the size-resolved fluorescence emission spectra (Figs. 6 and 7) depict a multimodal spectral profile at two sites. Spectra profile at each site is explained in terms of emission modes as a function of emission wavelength for both Xe1 and Xe2.

The available information on excitation-emission characteristics for a range of atmospherically relevant bio-fluorophores (Hernandez et al., 2016; Pöhlker et al., 2012; Hill et al., 2009; Pan et al., 2010) could help elucidate the molecular origin of fluorescence from biological materials and give an insight to deduce spectral modes to most likely

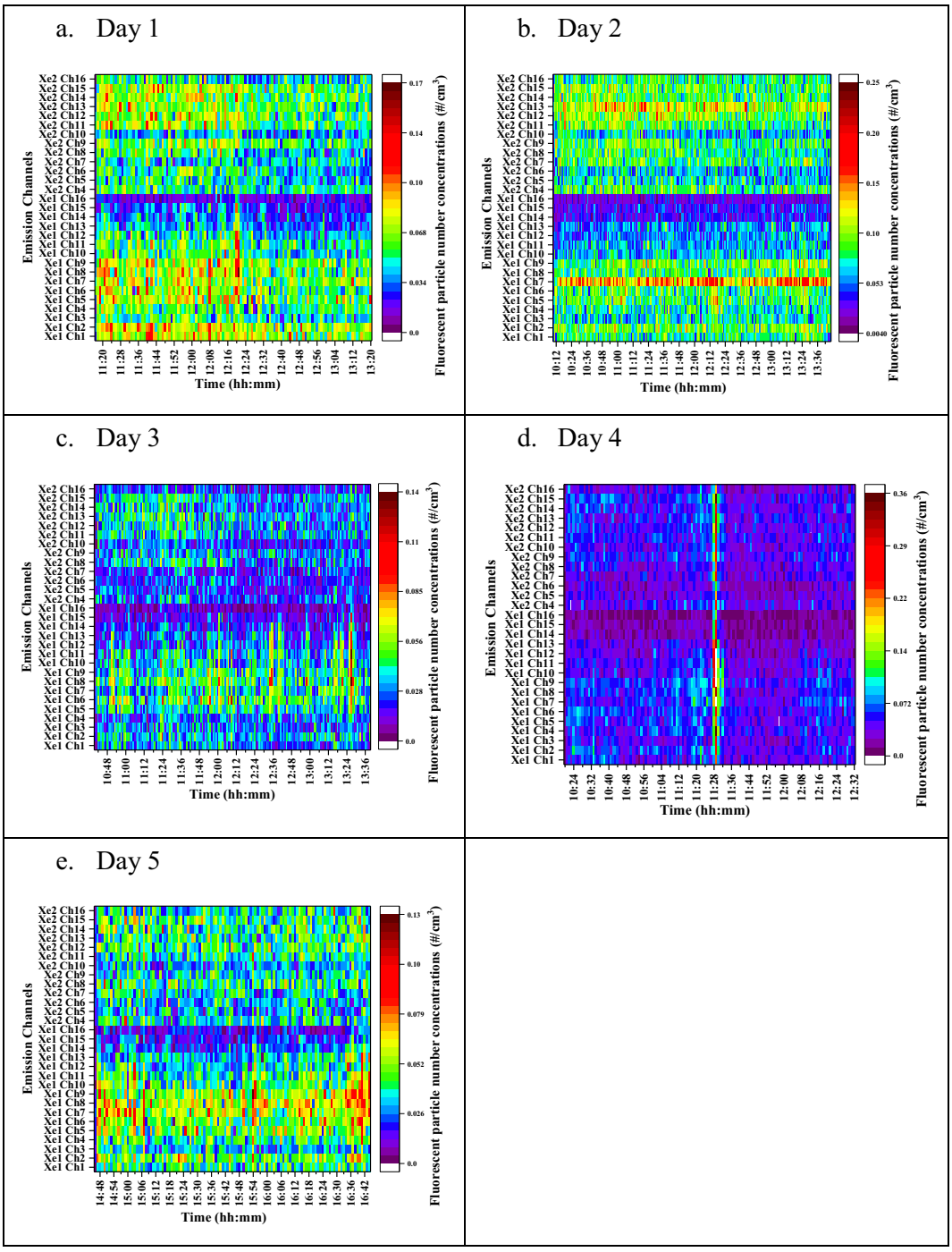

Fig. 5. Channel by channel number concentrations of fluorescent particles at the background site.

bio-fluorophores. Consequently, seven categories of potential bio-fluorophores in terms of their excitation and emission wavelengths relevant to SIBS were summarised following Pöhlker et al. (2012). Table 5 provides an overview of potential fluorophores with reference to SIBS excitation and emission wavelengths across various channels.

The overall spectra of the WWTP showed three major fluorescence peaks for excitation wavelength (λex) at 285 nm as follows in increasing order of emission wavelengths (λem): 316.4–344.8 nm (Ch2), 430.2–457.5 nm (Ch6), 486–514 nm (Ch8), along with a secondary peak at 652.8–680.2 nm (Ch14) (Fig. 6A). While for the excitation wavelength at 370 nm, two minor modes and one broad emission peak were observed at 430.2–457.5 nm (Ch6), 514.1–542 nm (Ch9) and 652.8–734.7 nm (Ch14–16). In contrast, the dominant and common peaks (Ch2 and Ch8 at λex = 285 nm; Ch9 and Ch15 at λex = 370 nm) of the background emission spectrum were comparable to the WWTP spectra (Fig. 6B). Moreover, the background spectrum had an emission peak at 401.5–429.7 nm (Ch5) at both excitation wavelengths. Additionally, the emission spectrum for 370 nm excitation had peaks at 569.9–597.6 nm (Ch11) and 625.3–652.8 nm (Ch13).

Among the overall spectra of two sites, the common emission modes could be assigned to tryptophan (amino acid-like), chlorophylls, lipofuscin and ceroid, bacteriochlorophyll, cellular age-related pigments and flavonoids (pigment-like), plant alkaloids, terpenoids, structurally smaller alkaloids (secondary metabolite-like), and chitin, sporopollenin (structural compound-like) fluorophores, which related to the presence of cellular fragments, bacteria, pollen and fungi. Moreover, pyridine

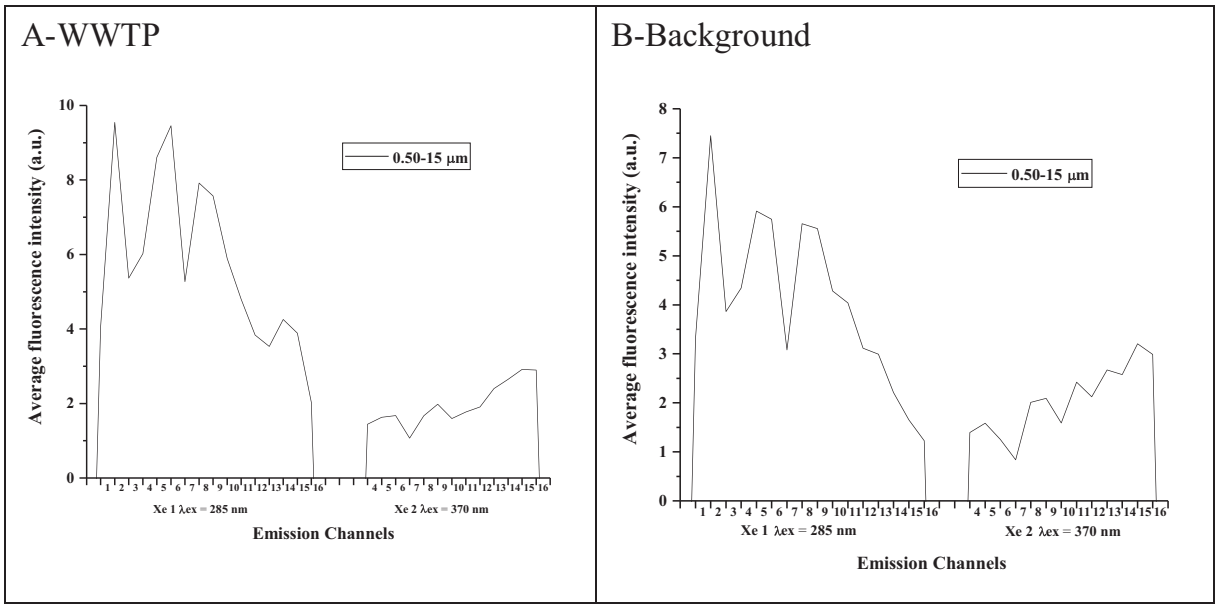

Fig. 6. Overall fluorescence spectra of (A) wastewater treatment plant and (B) background site.

nucleotides (coenzymes-like) fluorophore was only present in WWTP, which is a signal of active cell metabolite (Hairston et al., 1997). In contrast, vitamin B6 compounds, flavins (vitamins-like), cellulosic materials (structural compound-like), Calcium salt CaDPA (other fluorophores), phenolics (secondary metabolite-like) compounds could be assigned to the background spectra. HULIS (humic-/protein-acid like fluorescence) and PAHs could be assigned to both spectra, which were likely to be generated from dispersion of organic matter and fossil fuel emissions near the sampling site. Nasir et al. (2019) also analysed the fluorescence spectra at the WWTP. It was reported that a broad emission peak at 430.2–514 nm (Ch6–8) followed by a secondary peak at 597.6–625.2 nm (Ch12) and 680.3–707.5 nm (Ch15) for 280 nm excitation was observed (primary peaks at Ch2, Ch6, Ch8 and secondary peak at Ch14 in this study), while the emission spectrum for 370 nm excitation had peaks at 514–542 nm (Ch9), 597.6–652.8 nm (Ch12–13) and 680.3–707.5 nm (Ch15) (while Ch6, Ch9, Ch15 in this study). The emission modes and the assignment of fluorophores in these studies were comparable.

3.2.2. Size-resolved spectra profiles of WWTP and background site

For the size-segregated spectra at the WWTP (Fig. 7A–E), the peak fluorescence emission in 316.4–344.8 nm (Ch2) and 430.2–457.5 nm (Ch6) at λex = 285 nm, 514.1–542 nm (Ch9) at λex = 370 nm were found across each size ranges, and slight changes in modes were also observed. For instance, the 285 nm excitation spectra had a major peak in 514.1–542 nm (Ch9) when particles were <1 μm, while it shifted to 486–514 nm (Ch8) as the particle size increased. In addition, new modes also emerged in 652.8–680.2 nm (Ch14) for particle size 1–10 μm. Particles >2.5 μm reflected three emission peaks for the 370 nm excitation spectra, and small changes from 680.3–707.5 nm (Ch15) to 652.8–680.2 nm (Ch14) were found when particles were >4 μm. Moreover, it was found that the fluorescence intensity increased with the increase in particle size. This could be because fluorescence emission intensity is a function of particle size, and larger particles are likely to have fluorophores, capable of emitting plenty of photons to give integrated light intensity signal, thus a higher fluorescence intensity was recorded (Hill et al., 2001; Savage et al., 2017; Sivaprakasam et al., 2011). Furthermore, tryptophan, chitin, dipicolinic acid (DPA), flavonoids, plant alkaloids and sporopollenin fluorophores could be assigned to all the size ranges in terms of their common emission channels. While terpenoids fluorophore only assigned to particle sizing 1–10 μm, and chlorophyll and bacterio-chlorophyll fluorophores were potentially present in the particles with a diameter between 2.5 and 4 μm.

On the contrary, for the background site, there were complex patterns shown in the size-segregated spectra profile (Fig. 7A–E: background site). Only Ch5 at λex = 370 nm was consistently observed in the different size range. With reference to differences across different sizes, Ch2 (at λex = 285 nm) and Ch5 (at λex = 370 nm) were only present in 0.50 to 10 μm indicating the presence of structural compounds-like (e.g. chitin, cellulosic material), amino acids-like (e.g. tryptophan), and secondary metabolite-like (e.g. terpenoids, phenolics) fluorophores. While Ch11, Ch13, Ch15 (λex = 370 nm) were observed from 0.50 - 4 μm size range, which implied that pigments-like (e.g. chlorophyll, flavonoids, age-related pigments, lipofuscin and ceroid), secondary metabolite-like (e.g. terpenoids) and structural compounds-like (e.g. sporopollenin) fluorophores could be assigned into this particle size. Notably, there was no considerable increase in fluorescence intensity and number of modes with the increase in particle size in background spectra, which suggests more heterogeneity in the composition of biological materials at the WWTP in comparison to the background site. However, there was a clear shift of the primary fluorescence peak in 285 nm excitation spectra from Ch2 to Ch4 and Ch13 with an increase in particle size at background site (Fig. 7-E), which illustrates the dominant fluorophores changed from chitin, tryptophan to vitamin B6 compound, cellulose material, pigments and terpenoids categories.

Comparing size-segregated spectra at both sites in the same particle size range, differences were present in emission modes as well as assigned potential fluorophores. For size range 0.50–1 μm, Ch2 at λex = 285 nm and Ch5 at λex = 370 nm (amino acid-like, structural compound-like, secondary metabolite-like and vitamins-like

Table 4
Sample size of fluorescent particles for the analysis of fluorescence spectra (particle diameter: 0.50–15 μm) across different wavelength bands at each site.

Sites	Number of fluorescent particles					
	Sampling 1	Sampling 2	Sampling 3	Sampling 4	Sampling 5	Total
WWTP	115,126	50,976	40,065	196,009	40,974	443,150
Background	31,033	82,280	25,253	27,634	22,733	188,932

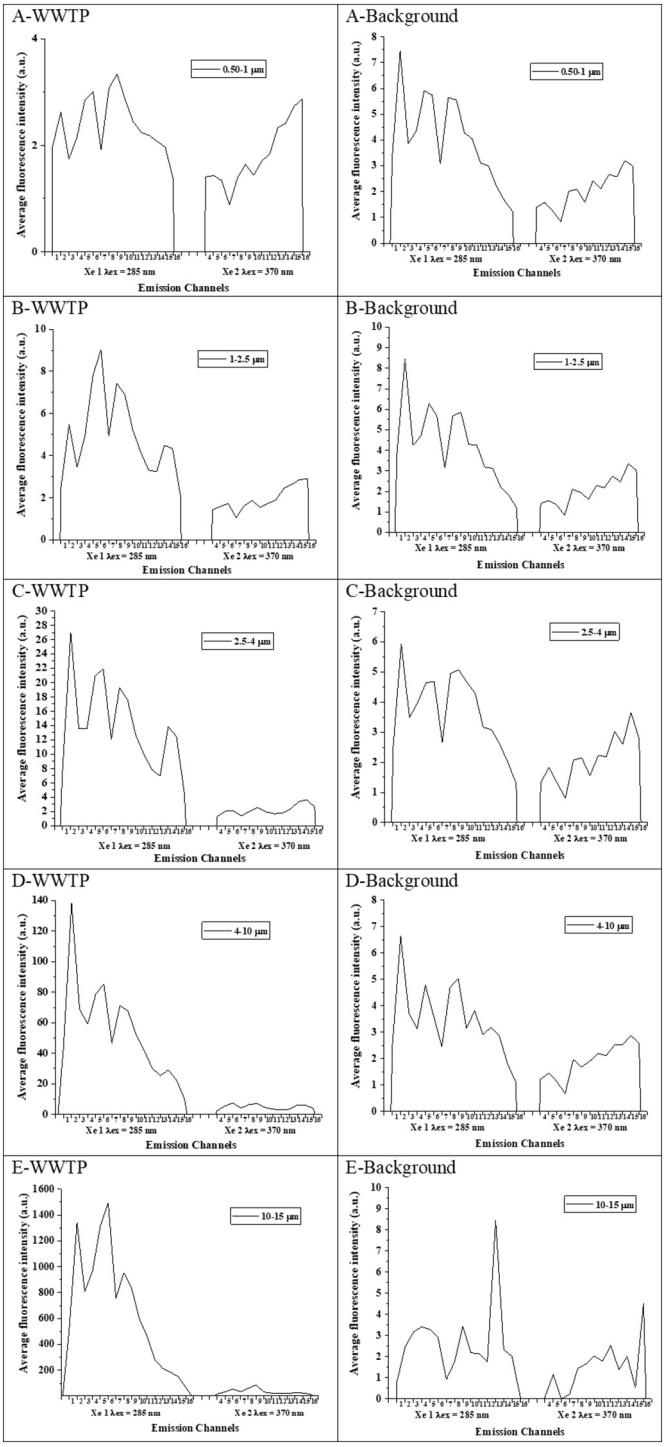

Fig. 7. Size-resolved fluorescence emission spectra profiles at WWTP (left) and background site (right). A: 0.50–1 μm, B: 1–2.5 μm, C: 2.5–4 μm, D: 4–10 μm, E: 10–15 μm.

fluorophores) were both common between WWTP and background site, but Ch11, Ch13, Ch15 at λex = 370 nm (mainly refer to pigment-like fluorophores) and Ch8 at λex = 285 nm (secondary metabolite-like fluorophores) only exhibited at background site. For particle size 1 to 2.5 μm, Ch2 (at λex = 285 nm) (e.g. tryptophan) was existing in both spectra, while Ch9 (at λex = 285 nm) (coenzymes-like, structural compound-like fluorophores) and Ch5, Ch8, Ch11, Ch13, Ch15 (at λex = 370) (pigments-like fluorophores) only exhibited in the background site. The commonality and differences between two sites for the size range of 2.5–4 μm were broadly similar to particles from 1 to 2.5 μm. The emission modes of 4–10 μm particles in both spectra were the most complicated, the primary peak for both spectra was located at Ch2. However, Ch6, Ch8, Ch14 (at λex = 285 nm) and Ch6, Ch9, Ch14 were only present in the WWTP spectra, and Ch5, Ch9, Ch11, Ch13 (at λex = 285 nm) and Ch5, Ch8, Ch11, Ch15 were only present in the background spectra. Particles between 10 and 15 μm showed that only Ch14 at λex = 370 nm was common between two sites, but there were considerable differences between the spectra at both sites.

Nevertheless, the comparison of emission intensity levels should be carefully applied as a semi-quantitative method, as fluorescence properties (e.g. spectral intensity) of a fluorophore are highly influenced by the molecular environment within biological cells or cellular fragments in atmospheric bioaerosols comparing to lab-based studies of pure fluorophores (Pöhlker et al., 2012; Pan, 2015). Additionally, the overlapping integrated fluorescence signals within each channel and the possible interfering non-biological compounds also make the discrimination of fluorophores challenging. Hence, lab-based studies with atmospherically relevant biological aerosols are required to build a comprehensive SIBS fluorescence spectra library. Such a library will greatly contribute to the elucidation of spectrally integrated signals and thus improve measurement selectivity for bioaerosol emissions (Nasir et al., 2019).

3.3. Excitation-emission matrix of wastewater samples

The comparison of SIBS fluorescence spectra from airborne particles and EEM of wastewater samples was performed to gain insights into the molecular origin of fluorescence and to improve assignment of SIBS spectral modes to known fluorophores. Fig. 8 demonstrates the EEM spectra of wastewater obtained from FluoroMax®-Plus. The highest fluorescence intensity area was centred at λex/λem = 285 nm / 340 nm (A. area), which is a typical signal of protein-like (containing tryptophan) fluorescence (Chen et al., 2003). As the most important contaminant in wastewater (Ahmad et al., 2002), it mainly originated from schoolyard domestic sewage, food residues and human faeces etc. within the university. The two secondary fluorescence peaks were concentrated at λex/λem = 260 nm / 430 nm (B. area) and λex/λem = 340 nm / 420 nm (C area), which belongs to the characteristic spectral position of humic acid and fulvic acid-like fluorescence (Coble, 1996). Humic acid is broadly existing in wastewater, being a significant component of natural organic matters (NOM) (Yamashita and Tanoue, 2003) that were generated by natural decay and subsequent atmospheric oxidation of biological material (Andreae and Gelencsér, 2006).

According to the assignment of possible fluorophores of SIBS spectra in Table 5, the three high fluorescence intensity areas probably cover amino acid-like (e.g. tryptophan, tyrosine), coenzyme-vitamins-like (e.g. pyridine nucleotides: NADH and NADPH, vitamin B6 compounds), structural compound-like (e.g. cellulose, chitin, lignin, sporopollenin), secondary metabolite-like (e.g. phenolics, terpenoids) bio-fluorophores. Those fluorophores reflected the presence of bacteria, fungi spores in the wastewater (e.g. Johansson and Lidén, 2006; Kopczynski et al., 2005; Lenardon et al., 2010; Wlodarski et al., 2006). Moreover, these emission modes (fluorophores) are broadly similar to the assignment fluorophores of SIBS resolved fluorescence spectra (Fig. 6A), which reveals that these compounds in wastewater are likely to be aerosolized into the ambient air at WWTP thus being detected by the SIBS. Furthermore, secondary organic aerosol (SOA) could be the non-biological compound since ammonia and nitrogen are rich in wastewater, and certain nitrogen-containing SOA was considered to be a vital source of autofluorescence (Bones et al., 2010). However, pigment-like fluorophores were hardly embraced in the EEM, which could explain that the pigment-like fluorophores within fluorescent aerosols detected by SIBS were mainly originated from natural materials (plants/grass), instead of aerosolization of wastewater.

There are several possible reasons for interpreting the similarity and difference between the SIBS spectra and wastewater EEM. Firstly, as a

Table 5
Overview of SIBS relevant excitation emission assignment to potential fluorophores.

Source/categories	Potential fluorophores	Excitation wavelength of SIBS (λex)	Corresponding SIBS emission channels	Fluorescence emission wavelength range (nm)	Reference
Amino acid	Tryptophan	Only at 285 nm	Ch2–3	340–353	Ramanujam (2000)
Cofactors, coenzymes, vitamins	Pyridine nucleotides: NADH and NADPH (Nicotinamide adenine dinucleotide (phosphate))	Both at 285 nm and 370 nm	Ch6–7	440–470	Billinton and Knight (2001)
	Flavins: Riboflavin, Flavin mononucleotide (FMN), Flavin adenine dinucleotide (FAD)	Both at 285 nm and 370 nm	Ch9–10	520–560	Pöhlker et al. (2012); Kopczynski et al. (2005)
	Vitamin B6 compounds: Pyridoxine, Pyridoxamine, Pyridoxal, 4-Pyridoxic acid, Pyridoxal-5′-phosphate	Both at 285 nm and 370 nm	Ch3–5	350–425	Pöhlker et al. (2012)
	Pteridine compounds: Folic acid (vitamin B9), Pterin, Biopterin, Neopterin, Lumazine	Only at 370 nm	Ch4–7	373–458	Kopczynski et al. (2005)
Structural biopolymers and cell wall compounds	Cellulosic materials	Both at 285 nm and 370 nm	Ch 4–5	−420	Castellan et al. (2007)
	Lignin	Both at 285 nm and 370 nm	Ch6–10	450–565	Pöhlker et al. (2012)
	Sporopollenin (mixture of fluorescent compounds (e.g., phenolics, carotenoids, azulene))	Only at 370 nm	Ch4–13	400–650	Roshchina (2003)
	Chitin	Only at 285 nm	Ch1–5	−410	Dreyer et al. (2006)
Pigments	Cellular age-related pigments	Both at 285 nm and 370 nm	Ch6–13	450–640	Andersson et al. (1998)
	Bacteriochlorophyll	at 370 nm	Ch15		Könemann et al. (2019)
	Chlorophyll a and b	Only at 370 nm	Ch13–16 (Ch14)	630–730	Könemann et al. (2019)
	Lipofuscin and ceroid	Both at 285 nm and 370 nm	Ch6–13	430–670	Eldred et al. (1982); Andersson et al. (1998)
	Flavonoids: e.g., anthocyanins, flavons, flavonols, isoflavones	Only at 370 nm	Ch6–12	440–610	Roshchina (2003); Roshchina and Mel'nikova (2001)
Secondary metabolites	Plant alkaloids	Only at 285 nm	Ch5–12	410–600	Roshchina (2003, 2005)
	Terpenoids: i.e. monoterpenes (e.g. menthol), sesquiterpenes (e.g. azulenes), diterpenes	Both at 285 nm and 370 nm	Ch5–16	400–725	Roshchina (2003)
	Phenolics	Both at 285 nm and 370 nm	Ch4–8	400–500	Roshchina et al. (2004)
	Structurally smaller alkaloids (e.g. atropine)	Only at 370 nm	Ch5–9	410–520	Pöhlker et al. (2012)
Other fluorophores (e.g., DNA and RNA as well as dipicolinic acid (DPA))	Calcium salt CaDPA	Only at 285 nm	Ch5	~−410	Alimova et al. (2003); Sarasanandarajah et al. (2005)
	DPA (pure, dry state)	Only at 285 nm	Ch6	~−440	Bronk et al. (2000)
	(HULIS) Humic-like fluorescence	Only at 370 nm	Ch4–8	400–500	Coble (1996); Hudson et al. (2007); Muller et al. (2008)
Potential interferences/non-biological fluorophores	Pure polycyclic aromatic hydrocarbons (PAHs)	Only at 370 nm	Ch5–8	310–540	Kumke et al. (1995)
	Several nitrogen-containing secondary organic aerosols (SOA)	Only at 285 nm	Ch5	420	Bones et al. (2010)

source of bioaerosol emission, wastewater and ambient air partly shared the same biological fractions. Secondly, the fluorescence properties of wastewater samples may be affected by the storage conditions or transport process, as well as the microbe's decay period. Thirdly, the air samples largely comprised of bioaerosols emitted from the ambient vegetation and were affected by the meteorological conditions and the operations of the wastewater treatment plant. In addition, the SIBS fluorescence emissions spectra were obtained from the average of all the fluorescent particles in every size range. There is need for developing advanced data analysis methods such as a clustering algorithm (e.g. hierarchical agglomerative cluster (HAC) analysis) (Crawford et al., 2015; Forde et al., 2018) to further elucidate bioaerosol emissions from WWTP utilising the highly resolved fluorescence intensity measurements of SIBS.

4. Conclusions

This study demonstrated that SIBS can provide real time and high-resolution signal for bioaerosols monitoring at WWTP and contribute to significantly advance the information on the nature and the magnitude of bioaerosols emission. The average level of NF and NT for bioaerosol emissions at the WWTP were higher than the

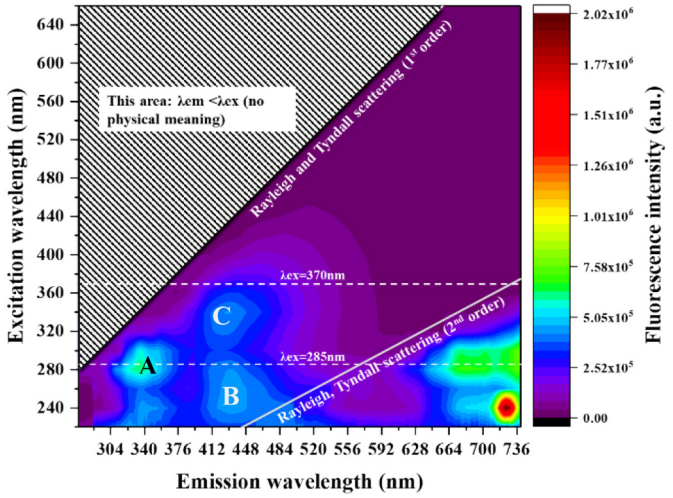

Fig. 8. Average excitation-emission matrix of five-day wastewater samples.

background site, and the temporal variation of NF and NT were highly variable and largely influenced by site-specific activities. In addition, the number-size distribution profile indicated the predominance of fine size particles (<1 μm) among fluorescent particles. Fluorescence emission spectra profiles were multimodal, and the assignment of the overall and size-segregated emission modes to existing SIBS relevant bio-fluorophores revealed the differences in fluorescence signature between the two sites. Moreover, the SIBS fluorescence spectra and EEM of the wastewater samples were broadly similar which demonstrates that SIBS can help to overcome the selectivity challenges to discriminate and classify bioaerosol emissions. Furthermore, the time-series channel-by-channel number concentration profile can provide a temporal variability of potential bio-fluorophores. However, it should be noted that SIBS is a beta version device therefore the data analysis capability is limited in its present form. Although the size-segregated fluorescence spectra appear to be different in emission modes there is a need for further analysis of time-dependent size-segregated SIBS spectra to give insight into what emission channels (or bio-fluorophores) are more dominant under a short time period and how it changes along with the time. Finally, the fluorescence threshold in each channel has been determined as the average + 3σ of FT fluorescence intensity measurements. This method assumes that FT fluorescence intensity among different channels of the SIBS is normally distributed. However, the fluorescence intensity may not be normally distributed in all the channels. Alternative approaches to set the fluorescence threshold should be further developed. With reference to the development of data analysis approaches, the existing data analytics being developed for WIBS (Crawford et al., 2015; Forde et al., 2018, Ruske et al., 2018) need to be explored for the SIBS specific data analysis tools.

CRediT authorship contribution statement

Jiang-han Tian: Data curation, Formal analysis, Investigation, Methodology, Visualization, Writing - original draft, Writing - review & editing.**Cheng Yan:**Conceptualization, Data curation, Formal analysis, Investigation, Methodology, Supervision, Visualization, Writing - review & editing.**Zaheer Ahmad Nasir:**Conceptualization, Data curation, Formal analysis, Investigation, Methodology, Resources, Supervision, Visualization, Writing - review & editing.**Sonia Garcia Alcega:**Writing - review & editing.**Sean Tyrrel:**Resources, Writing - review & editing. **Frederic Coulon:**Conceptualization, Resources, Supervision, Writing - review & editing.

Declaration of competing interest

The authors declare that they have no known competing financial interests or personal relationships that could have appeared to influence the work reported in this paper.

Acknowledgements

The authors acknowledge the financial support from the UK Natural Environment Research Council (NERC) through the Environmental Microbiology and Human Health Programme (Grant Reference NE/M01163/1 and NE/M010961/1). Cheng Yan's academic visit at Cranfield University was supported by the National Natural Science Foundation of China (51608497). The underlying data can be accessed at https://doi.org/10.17862/cranfield.rd.11663313.v1.

Appendix A. Supplementary data

Supplementary data to this article can be found online at https://doi.org/10.1016/j.scitotenv.2020.137629.

References

Ahmad, U.K., Ujang, Z., Yusop, Z., Fong, T.L., 2002. Fluorescence technique for the characterization of natural organic matter in river water. Water Sci. Technol. 46 (9), 117–125.
Alimova, A., Katz, A., Savage, H.E., Shah, M., Minko, G., Will, D.V., Alfano, R.R., 2003. Native fluorescence and excitation spectroscopic changes in Bacillus subtilis and Staphylococcus aureus bacteria subjected to conditions of starvation. Appl. Opt. 42 (19), 4080–4087.
Andersson, H., Baechi, T., Hoechl, M., Richter, C., 1998. Autofluorescence of living cells. J. Microsc. 191, 1–7 Pt 1.
Andreae, M.O., Gelencsér, A., 2006. Black carbon or brown carbon? The nature of light-absorbing carbonaceous aerosols. Atmos. Chem. Phys. 6 (10), 3131–3148.
Billinton, N., Knight, A.W., 2001. Seeing the wood through the trees: a review of techniques for distinguishing green fluorescent protein from endogenous autofluorescence. Anal. Biochem. 291 (2), 175–197.
Bones, D.L., Henricksen, D.K., Mang, S.A., Gonsior, M., Bateman, A.P., Nguyen, T.B., Nizkorodov, S.A., 2010. Appearance of strong absorbers and fluorophores in limonene-O3 secondary organic aerosol due to NH4+-mediated chemical aging over long time scales. Journal of Geophysical Research: Atmospheres 115 (D5).
Bowers, R.M., Lauber, C.L., Wiedinmyer, C., Hamady, M., Hallar, A.G., Fall, R., Fierer, N., 2009. Characterization of airborne microbial communities at a high-elevation site and their potential to act as atmospheric ice nuclei. Appl. Environ. Microbiol. 75 (15), 5121–5130.
Bronk, B.V., Shoaibi, A., Nudelman, R., Akinyemi, A.N., 2000. Physical perturbation for fluorescent characterization of microorganism particles. Chemical and Biological Sensing. 4036. International Society for Optics and Photonics, pp. 169–180.
Castellan, A., Ruggiero, R., Frollini, E., Ramos, L.A., Chirat, C., 2007. Studies on fluorescence of cellulosics. Holzforschung 61 (5), 504–508.
Chen, W., Westerhoff, P., Leenheer, J.A., Booksh, K., 2003. Fluorescence excitation-emission matrix regional integration to quantify spectra for dissolved organic matter. Environ. Sci. Technol. 37 (24), 5701–5710.
Chi, M.C., Li, C.S., 2007. Fluorochrome in monitoring atmospheric bioaerosols and correlations with meteorological factors and air pollutants. Aerosol Sci. Technol. 41 (7), 672–678.
Clauß, M., 2015. Particle size distribution of airborne micro-organisms in the environment-a review. Landbauforsch Appl Agric Forestry Res 65, 77–100.
Coble, P.G., 1996. Characterization of marine and terrestrial dom in seawater using excitation-emission matrix spectroscopy. Mar. Chem. 51 (4), 325–346.
Crawford, I., Ruske, S., Topping, D.O., Gallagher, M.W., 2015. Evaluation of hierarchical agglomerative cluster analysis methods for discrimination of primary biological aerosol. Atmos. Meas. Tech. 8 (11), 4979–4991.
Crawford, I., Lloyd, G., Herrmann, E., Hoyle, C.R., Bower, K.N., Connolly, P.J., Gallagher, M.W., 2016. Observations of fluorescent aerosol–cloud interactions in the free troposphere at the High-Altitude Research Station Jungfraujoch. Atmos. Chem. Phys. 16 (4), 2273–2284.
Després, V.R., Nowoisky, J.F., Klose, M., Conrad, R., Andreae, M.O., Pöschl, U., 2007. Characterization of primary biogenic aerosol particles in urban, rural, and high-alpine air by DNA sequence and restriction fragment analysis of ribosomal RNA genes. Biogeosciences 4 (6), 1127–1141.
Dreyer, B., Morte, A., Pérez-Gilabert, M., Honrubia, M., 2006. Autofluorescence detection of arbuscular mycorrhizal fungal structures in palm roots: an underestimated experimental method. Mycol. Res. 110 (8), 887–897.
Eldred, G.E., Miller, G.V., Stark, W.S., Feeney-Burns, L., 1982. Lipofuscin: resolution of discrepant fluorescence data. Science 216 (4547), 757–759.
Ferguson, R.M., Garcia-Alcega, S., Coulon, F., Dumbrell, A.J., Whitby, C., Colbeck, I., 2019. Bioaerosol biomonitoring: sampling optimization for molecular microbial ecology. Mol. Ecol. Resour. 19 (3), 672–690.

Forde, E., Gallagher, M., Foot, V., Sarda, R., Crawford, I., Kaye, P., Stanley, W., Topping, D., 2018. Characterisation of biofluorescent aerosol emissions over winter and summer periods in the United Kingdom. Atmos. Chem. Phys. 1–31.
Fracchia, L., Pietronave, S., Rinaldi, M., Martinotti, M.G., 2006. Site-related airborne biological hazard and seasonal variations in two wastewater treatment plants. Water Res. 40 (10), 1985–1994.
Fröhlich-Nowoisky, J., Pickersgill, D.A., Després, V.R., Pöschl, U., 2009. High diversity of fungi in air particulate matter. Proc. Natl. Acad. Sci. 106 (31), 12814–12819.
Gabey, A.M., Vaitilingom, M., Freney, E., Boulon, J., Sellegri, K., Gallagher, M.W., Kaye, P.H., 2013. Observations of fluorescent and biological aerosol at a high-altitude site in central France. Atmos. Chem. Phys. 13 (15), 7415–7428.
Galès, A., Bru-Adan, V., Godon, J.J., Delabre, K., Catala, P., Ponthieux, A., Wéry, N., 2015. Predominance of single bacterial cells in composting bioaerosols. Atmos. Environ. 107, 225–232.
Garcia-Alcega, S., Nasir, Z.A., Ferguson, R., Whitby, C., Dumbrell, A.J., Colbeck, I., Coulon, F., 2017. Fingerprinting outdoor air environment using microbial volatile organic compounds (MVOCs)—a review. TrAC Trends Anal. Chem. 86, 75–83.
Garcia-Alcega, S., Nasir, Z.A., Ferguson, R., Noël, C., Cravo-Laureau, C., Whitby, C., Coulon, F., 2018. Can chemical and molecular biomarkers help discriminate between industrial, rural and urban environments? Sci. Total Environ. 631, 1059–1069.
Gerardi, M.H., Zimmerman, M.C., 2004. Wastewater Pathogens. John Wiley and Sons.
Gilmore, A.M., 2011. Water quality measurements with HORIBA Jobin Yvon fluorescence instrumentation. Readout 38, 90–96.
Griffiths, W.D., DeCosemo, G.A.L., 1994. The assessment of bioaerosols: a critical review. J. Aerosol Sci. 25 (8), 1425–1458.
Hairston, P.P., Ho, J., Quant, F.R., 1997. Design of an instrument for real-time detection of bioaerosols using simultaneous measurement of particle aerodynamic size and intrinsic fluorescence. J. Aerosol Sci. 28, 471–482.
Healy, D.A., Huffman, J.A., O'Connor, D.J., Pöhlker, C., Pöschl, U., Sodeau, J.R., 2014. Ambient measurements of biological aerosol particles near Killarney, Ireland: a comparison between real-time fluorescence and microscopy techniques. Atmos. Chem. Phys. 14, 8055–8069.
Heidelberg, J.F., Shahamat, M., Levin, M., Rahman, I., Stelma, G., Grim, C., Colwell, R.R., 1997. Effect of aerosolization on culturability and viability of gram-negative bacteria. Appl. Environ. Microbiol. 63 (9), 3585–3588.
Hernandez, M., Perring, A.E., McCabe, K., Kok, G., Granger, G., Baumgardner, D., 2016. Chamber catalogues of optical and fluorescent signatures distinguish bioaerosol classes. Atmospheric Measurement Techniques 9 (7).
Hill, S.C., Pinnick, R.G., Niles, S., Fell, N.F., Pan, Y.L., Bottiger, J., Chang, R.K., 2001. Fluorescence from airborne microparticles: dependence on size, concentration of fluorophores, and illumination intensity. Appl. Opt. 40 (18), 3005–3013.
Hill, S.C., Mayo, M.W., Chang, R.K., 2009. Fluorescence of Bacteria, Pollens, and Naturally Occurring Airborne Particles: Excitation/Emission Spectra (No. ARL-TR-4722). Army Research Lab Adelphi Md Computational and Information Sciences Directorate.
Horiba, 2009. FluoroMax®-4 and FluoroMax®-4P With USB Operation Manual Part Number 810005 Version B. HORIBA Jobin Yvon Inc.
Horiba, 2012. FluorEssence 3.5 User's Guide Rev. C (26 Jan 2012). HORIBA Instruments Incorporated.
Hudson, N., Baker, A., Reynolds, D., 2007. Fluorescence analysis of dissolved organic matter in natural, waste and polluted waters—a review. River Res. Appl. 23 (6), 631–649.
Huffman, J.A., Treutlein, B., Pöschl, U., 2010. Fluorescent biological aerosol particle concentrations and size distributions measured with an Ultraviolet Aerodynamic Particle Sizer (UV-APS) in Central Europe. Atmos. Chem. Phys. 10 (7), 3215–3233.
Huffman, J.A., Sinha, B., Garland, R.M., Snee-Pollmann, A., Gunthe, S.S., Artaxo, P., Pöschl, U., 2012. Size distributions and temporal variations of biological aerosol particles in the Amazon rainforest characterized by microscopy and real-time UV-APS fluorescence techniques during AMAZE-08. Atmos. Chem. Phys. 12 (24), 11997–12019.
Huffman, J.A., Perring, A.E., Savage, N.J., Clot, B., Crouzy, B., Tummon, F., Shoshanim, O., Damit, B., Schneider, J., Sivaprakasam, V., Zawadowicz, M.A., 2019. Real-time sensing of bioaerosols: Review and current perspective. Aerosol Sci. Technol. https://doi.org/10.1080/02786826.2019.1664724.
IWA, 2018. The Reuse Opportunity. Wastewater Report 2018. The international water association. Alliance House, 12 Caxton Street, London SW1H 0QS, UK.
Johansson, L., Lidén, G., 2006. A study of long-term effects on plasmid-containing Escherichia coli in carbon-limited chemostat using 2D-fluorescence spectrofluorometry. Biotechnol. Prog. 22 (4), 1132–1139.
Könemann, T., Savage, N., Klimach, T., Walter, D., Fröhlich-Nowoisky, J., Su, H., Pöhlker, C., 2019. Spectral Intensity Bioaerosol Sensor (SIBS): an instrument for spectrally resolved fluorescence detection of single particles in real time. Atmospheric Measurement Techniques 12 (2), 1337–1363.
Kopczynski, K., Kwasny, M., Mierczyk, Z., Zawadzki, Z., 2005. Laser induced fluorescence system for detection of biological agents: European project FABIOLA. Optical Security Systems. 5954. International Society for Optics and Photonics, p. 595405.
Korzeniewska, E., 2011. Emission of bacteria and fungi in the air from wastewater treatment plants - a review. Frontiers in Bioscience - Scholar 3 S (2), 393–407.
Korzeniewska, E., Filipkowska, Z., Gotkowska-Płachta, A., Janczukowicz, W., Rutkowski, B., 2008. Bacteriological pollution of the atmospheric air at the municipal and dairy wastewater treatment plant area and in its surroundings. Archives of Environmental Protection 34 (4), 13–23.
Kowalski, M., Pastuszka, J.S., 2018. Effect of ambient air temperature and solar radiation on changes in bacterial and fungal aerosols concentration in the urban environment. Annals of Agricultural and Environmental Medicine 25 (2), 259–261.
Kumke, M.U., Löhmannsröben, H.G., Roch, T., 1995. Fluorescence spectroscopy of polynuclear aromatic compounds in environmental monitoring. J. Fluoresc. 5 (2), 139–152.
Lenardon, M.D., Munro, C.A., Gow, N.A., 2010. Chitin synthesis and fungal pathogenesis. Curr. Opin. Microbiol. 13 (4), 416–423.
Li, J., Zhou, L., Zhang, X., Xu, C., Dong, L., Yao, M., 2016. Bioaerosol emissions and detection of airborne antibiotic resistance genes from a wastewater treatment plant. Atmos. Environ. 124, 404–412.
Mateo-Sagasta, J., Raschid-Sally, L., Thebo, A., 2015. Global wastewater and sludge production, treatment and use. Wastewater. Springer, Dordrecht, pp. 15–38.
Miao, H., Rubakhin, S.S., Sweedler, J.V., 2003. Analysis of serotonin release from single neuron soma using capillary electrophoresis and laser-induced fluorescence with a pulsed deep-UV NeCu laser. Anal. Bioanal. Chem. 377 (6), 1007–1013.
Michałkiewicz, M., 2019. Wastewater treatment plants as a source of bioaerosols. Pol. J. Environ. Stud. 28 (4), 2261–2271.
Muller, C.L., Baker, A., Hutchinson, R., Fairchild, I.J., Kidd, C., 2008. Analysis of rainwater dissolved organic carbon compounds using fluorescence spectrophotometry. Atmos. Environ. 42 (34), 8036–8045.
Nasir, Z., Rolph, C., Collins, S., Stevenson, D., Gladding, T., Hayes, E., Parks, S., 2018. A controlled study on the characterisation of bioaerosols emissions from compost. Atmosphere 9 (10), 379.
Nasir, Z.A., Hayes, E., Williams, B., Gladding, T., Rolph, C., Khera, S., Tyrrel, S., 2019. Scoping studies to establish the capability and utility of a real-time bioaerosol sensor to characterise emissions from environmental sources. Sci. Total Environ. 648, 25–32.
O'Connor, D.J., Daly, S.M., Sodeau, J.R., 2015. On-line monitoring of airborne bioaerosols released from a composting/green waste site. Waste Manag. 42, 23–30.
Pan, Y.L., 2015. Detection and characterization of biological and other organic-carbon aerosol particles in atmosphere using fluorescence. J. Quant. Spectrosc. Radiat. Transf. 150, 12–35.
Pan, Y.L., Hill, S.C., Pinnick, R.G., Huang, H., Bottiger, J.R., Chang, R.K., 2010. Fluorescence spectra of atmospheric aerosol particles measured using one or two excitation wavelengths: comparison of classification schemes employing different emission and scattering results. Opt. Express 18 (12), 12436–12457.
Pascual, L., Pérez-Luz, S., Yáñez, M.A., Santamaría, A., Gibert, K., Salgot, M., Catalán, V., 2003. Bioaerosol emission from wastewater treatment plants. Aerobiologia 19 (3–4), 261–270.
Perring, A.E., Schwarz, J.P., Baumgardner, D., Hernandez, M.T., Spracklen, D.V., Heald, C.L., Fahey, D.W., 2015. Airborne observations of regional variation in fluorescent aerosol across the United States. J. Geophys. Res. 120, 1153–1170.
Pöhlker, C., Huffman, J.A., Pöschl, U., 2012. Autofluorescence of atmospheric bioaerosols - fluorescent biomolecules and potential interferences. Atmospheric Measurement Techniques 5 (1), 37–71.
Prazmo, Z., Krysinska-Traczyk, E., Skorska, C., Sitkowska, J., Cholewa, G., Dutkiewicz, J., 2003. Exposure to bioaerosols in a municipal sewage treatment plant. Annals of agricultural and environmental medicine: AAEM 10 (2), 241–248.
Ramanujam, N., 2000. Fluorescence spectroscopy of neoplastic and non-neoplastic tissues. Neoplasia 2 (1–2), 89–117.
Rizzo, L., Manaia, C., Merlin, C., Schwartz, T., Dagot, C., Ploy, M.C., Michael, I., Fatta- Kassinos, D., 2013. Urban wastewater treatment plants as hotspots for antibiotic resistant bacteria and genes spread into the environment: a review. Sci. Total Environ. 447, 345–360.
Roshchina, V.V., 2003. Autofluorescence of plant secreting cells as a biosensor and bioindicator reaction. J. Fluoresc. 13 (5), 403–420.
Roshchina, V.V., 2005. Allelochemicals as fluorescent markers, dyes and probes. Allelopathy J 16 (1), 31–46.
Roshchina, V.V., Mel'nikova, E.V., 2001. Pollen chemosensitivity to ozone and peroxides. Russ. J. Plant Physiol. 48 (1), 74–83.
Roshchina, V.V., Yashin, V.A., Kononov, A.V., 2004. Autofluorescence of developing plant vegetative microspores studied by confocal microscopy and microspectrofluorimetry. J. Fluoresc. 14 (6), 745–750.
Ruske, S., Topping, D.O., Foot, V.E., Morse, A.P., Gallagher, M.W., 2018. Machine learning for improved data analysis of biological aerosol using the WIBS. Atmospheric Measurement Techniques 11 (11), 6203–6230.
Sarasanandarajah, S., Kunnil, J., Bronk, B.V., Reinisch, L., 2005. Two-dimensional multiwavelength fluorescence spectra of dipicolinic acid and calcium dipicolinate. Appl. Opt. 44 (7), 1182–1187.
Savage, N.J., Krentz, C.E., Könemann, T., Han, T.T., Mainelis, G., Pöhlker, C., Huffman, J.A., 2017. Systematic characterization and fluorescence threshold strategies for the wideband integrated bioaerosol sensor (WIBS) using size-resolved biological and interfering particles. Atmospheric Measurement Techniques 10 (11), 4279–4302.
Sivaprakasam, V., Lin, H.B., Huston, A.L., Eversole, J.D., 2011. Spectral characterization of biological aerosol particles using two-wavelength excited laser-induced fluorescence and elastic scattering measurements. Opt. Express 19 (7), 6191–6208.
Swan, J.R.M., Kelsey, A., Crook, B., Gilbert, E.J., 2003. Occupational and Environmental Exposure to Bioaerosols From Composts and Potential Health Effects: A Critical Review of Published Data. 130. HSE Books, Sudbury.
Wlodarski, M., Kaliszewski, M., Kwasny, M., Kopczynski, K., Zawadzki, Z., Mierczyk, Z., Szpakowska, M., 2006. Fluorescence excitation-emission matrices of selected biological materials. Optically Based Biological and Chemical Detection for Defence III. 6398. International Society for Optics and Photonics, p. 639806.
Yamashita, Y., Tanoue, E., 2003. Chemical characterization of protein-like fluorophores in DOM in relation to aromatic amino acids. Mar. Chem. 82, 255–271.
Yue, S., Ren, L., Song, T., Li, L., Xie, Q., Li, W., Sun, Y., 2019. Abundance and diurnal trends of fluorescent bioaerosols in the troposphere over Mt. Tai, China, in spring. Journal of Geophysical Research: Atmospheres 124 (7), 4158–4173.
Zhong, X., Qi, J., Li, H., Dong, L., Gao, D., 2016. Seasonal distribution of microbial activity in bioaerosols in the outdoor environment of the Qingdao coastal region. Atmos. Environ. 140, 506–513.
Ziemba, L.D., Beyersdorf, A.J., Chen, G., Corr, C.A., Crumeyrolle, S.N., Diskin, G., Shook, M., 2016. Airborne observations of bioaerosol over the Southeast United States using a wideband integrated bioaerosol sensor. Journal of Geophysical Research: Atmospheres 121 (14), 8506–8524.